SLC25A1 reprograms mitochondrial and fatty acid metabolism to promote the progression of acute myeloid leukemia

Miao Chen,[1*] Wenze Li,[1*] Yuan Tao,[1*] Chenglong Hu,[2] Rui Ge,[1] Sijing Kang,[1] Pengjie Yue,[1] Cheuk Him Man,[3] Lan Wang[2#] and Xiaojing Yan[1#]

[1]Department of Hematology, The First Affiliated Hospital of China Medical University, Shenyang; [2]CAS Key Laboratory of Tissue Microenvironment and Tumor, Shanghai Institute of Nutrition and Health, Shanghai Institutes for Biological Sciences, University of Chinese Academy of Sciences, Chinese Academy of Sciences, Shanghai and [3]Department of Medicine, Li Ka Shing Faculty of Medicine, The University of Hong Kong, Hong Kong SAR, China

**MC, WL and YT contributed equally as first authors.*
#LW and XY contributed equally as senior authors.

Correspondence: X. Yan
yanxiaojing_pp@hotmail.com
L. Wang
lwang@sinh.ac.cn

Received: January 6, 2025.
Accepted: August 7, 2025.
Early view: September 4, 2025.

https://doi.org/10.3324/haematol.2024.287269

Supplementary Figure Legends

Supplementary Figure 1. SLC25A1 expression profiling in AML cell lines. (A) The gene effect (chronos) of SLC25A1 knockout in various AML cell lines from DEPMAP CRISPR database. (B) The qPCR analysis of SLC25A1 expression in BM mononuclear cells from healthy donors (n=15) and AML (except M3) patients (n=69); qPCR analysis of SLC2511A1 expression in BM mononuclear cells from healthy donors (n=15) and AML patients of various subtypes, including AML1-ETO (n=11), MLL-AF9 (n=2), CBFB-MYH11 (n=3) and subtype with no fusion genes (n=39). (C) The positive ratio of SLC25A1 protein expression in BM mononuclear cells from healthy donors (n=3) and AML patients (n=3) (D) The mRNA expression of SLC25A1 in various AML cell lines from DEPMAP database. (E) The protein expression of SLC25A1 in various AML cell lines from DEPMAP database. (F) The expression levels of SLC25A1 in leukemia stem cell- negative (LSC^-) and LSC- positive (LSC^+) fractions from two independent AML datasets: GSE76009 (left) and GSE230423 (right).

Supplementary Figure 2. SLC25A1 has no effect on AML cell cycle and differentiation. (A) The RNA and protein expression of SLC25A1 was knockdown after shSLC25A1 lentiviruses transfection in Kasumi-1 and THP1 cells. (B) The colony formation assay of Kasumi-1 and THP1 cells after SLC25A1 knockdown with shControl, shSLC25A1-1 and shSLC25A1-2 lentiviruses. (C) The percentage of apoptotic leukemia cells at day 2 after SLC25A1 knockdown. (D)The cell cycle was not affected after SLC25A1 knockdown in Kasumi-1 and THP1 cells. (E) The cell

differentiation was not affected after SLC25A1 knockdown in Kasumi-1 and THP1 cells. (F) The colony formation assay of human primary AML cells (AML#5) after SLC25A1 knockdown with shControl, shSLC25A1-1 and shSLC25A1-2 lentiviruses. (G) The growth of MOLM14 and OCIAML2 cells was inhibited after SLC25A1 knockdown with shControl and shSLC25A1-2 lentiviruses.

Supplementary Figure 3. SLC25A1 KD has no effect on HL60 cells. (A) The RNA and protein expression of SLC25A1 was knockdown after shSLC25A1-1 and shSLC25A1-2 lentiviruses transfection in HL60 cells. The growth of HL60 cells was not affected after SLC25A1 knockdown. (B) The colony formation assay of HL60 cells after SLC25A1 knockdown. (C) The percentage of apoptotic leukemia cells was not affected at day 2 after SLC25A1 knockdown. (D) The cell cycle was not affected after SLC25A1 knockdown in HL60 cells. (E) The cell differentiation was not affected after SLC25A1 knockdown in HL60 cells. (F) The RNA expression of SLC25A1 was overexpression after ovSLC25A1 lentiviruses transfection in HL60. The growth of HL60 cells was promoted after SLC25A1 overexpression with ov-SLC25A1 lentiviruses. (G) The colony formation assay of HL60 cells after SLC25A1 overexpression with ovSLC25A1-1 lentiviruses. (H) The cell cycle was not affected after SLC25A1 overexpression in HL60 cells. (I) The cell differentiation was not affected after SLC25A1 overexpression in HL60 cells.

Supplementary Figure 4. SLC25A1 inhibitor (CTPI2) inhibits the growth of AML cells but has no effect on mononuclear cells from healthy bone marrow. (A) The

colony formation assay of Kasumi-1 and THP1 cells after CTPI2 application. (B) The growth of MOLM14 and OCIAML2 cells was inhibited after CTPI2 application. (C) The growth of human primary AML cells (AML#1, #2, #4, #5) was inhibited after CTPI2 application, but the growth of mononuclear cells from healthy bone marrow was not affected by CTPI2. (D) The percentage of apoptotic leukemia cells at day 1 after CTPI2 application.

Supplementary Figure 5. SLC25A1 knockdown inhibits the growth of murine AML cells in vitro and vivo. (A) The RNA and protein expression of SLC25A1 was knockdown after shSLC25A1 lentiviruses transfection in AE9a and MLL-AF9 cells. (B) The growth of AE9a and MLL-AF9 cells was inhibited after CTPI2 application. (C) The RNA and protein expression of SLC25A1 was knockdown after shSLC25A1 lentiviruses transfection in AE9a LSCs and MLL-AF9 LGMP cells. (D) The colony formation assay of AE9a LSCs and MLL-AF9 LGMPs after SLC25A1 knockdown. (E) The size changes of the spleen and liver and the weight changes of the liver in recipient mice transplanted with AE9a cells after SLC25A1 knockdown. (F) The frequencies of $GFP^{+}c\text{-}Kit^{+}$ or $GFP^{+}Mac1^{-}$ leukemia blast cells in the bone marrow, the spleen and the peripheral blood of recipient mice transplanted with shControl AE9a cells and shSLC25A1 AE9a cells. (G) The HE staining analysis of bone marrow and spleen isolated from recipient mice transplanted with shControl AE9a cells and shSLC25A1 AE9a cells.

Supplementary Figure 6. SLC25A1 KD impairs the function of mitochondria and elevates the cellular ROS level. (A) The change of mitochondrial membrane potential through fluorescence microscope after SLC25A1 knockdown or CTPI2 application in Kasumi-1 and THP1 cells. (B) The change of mitochondrial membrane potential through flow cytometry after SLC25A1 knockdown or CTPI2 application in Kasumi-1 and THP1 cells. (C) The change of mitochondrial membrane potential measured by fluorescence microscope after SLC25A1 knockdown or CTPI2 application in Kasumi-1, THP1 cells. (D) The OCRs measured by seahorse extracellular flux analyzer experiment after SLC25A1 knockdown and CTPI2 application in THP1. (E) The cellular ROS levels measured by flow cytometry after SLC25A1 knockdown and CTPI2 application in THP1. (F) The cellular ROS levels measured by fluorescence microscope after SLC25A1 knockdown or CTPI2 application in Kasumi-1, THP1 cells. (G) The growth of AML cells is rescued by ROS remover (NAC) in Kasumi-1 and THP1 transfected with shSLC25A1 and CTPI2 application.

Supplementary Figure 7. The synergistic effect of CTPI2 with venetoclax on inhibiting the growth and promoting the apoptosis in AML cells. (A) The growth of Kasumi-1 and THP1 cells with shControl or shSLC25A1 after venetoclax application. (B) The synergistic effect of CTPI2 and venetoclax on inhibiting the growth of Kasumi-1 and THP1 cells. (C) The synergistic effect of CTPI2 and venetoclax on promoting the apoptosis of Kasumi-1 and THP1 cells. (D) The synergistic effect of CTPI2 and venetoclax on elevating the ROS level of Kasumi-1 cells.

Supplementary Figure 8. SLC25A1 significantly affects fatty acid metabolism in AML cells. (A) The GO enrichment analysis of SLC25A1 related genes (R>0.5) in TCGA AML RNA sequencing database. (B) The GO enrichment analysis of SLC25A1 related genes (R>0.5) in Vizome AML RNA sequencing database. (C) The GO enrichment analysis of DEGs performed by RNA sequencing on Kasumi-1 with SLC25A1 knockdown. The GSEA performed by RNA sequencing on Kasumi-1 with SLC25A1 knockdown indicating SLC25A1 is correlated with apoptosis pathway and oxidative phosphorylation. (D) The GSEA performed by RNA sequencing on Kasumi-1 with SLC25A1 knockdown indicating SLC25A1 is correlated with fatty acid homeostasis. (E) The protein-protein interaction network of SLC25A1 by STRING online tool. (F) The protein-protein interaction network of SLC25A1 by GeneMANIA online tool. (G) The correlation curves of SLC25A1 expression and ACLY expression, or FASN expression in TCGA AML RNA sequencing database. (H) The correlation curves of SLC25A1 expression and ACLY expression, or FASN expression in Vizome AML RNA sequencing database. (I) The WB validation of SLC25A1 KD on the expression of CPT1A, CPT1C in Kasumi-1 and CPT1A, CPT1C, ACLY, FASN in THP1 cells. (J) The protein expression of CPT1A and CPT1C by three times WB after SLC25A1 knockdown in Kasumi-1 and THP1 cells. The protein expression of ACLY and FASN by three times WB after SLC25A1 knockdown in Kasumi-1 and THP1 cells. (K) The change of citrate level detected by metabolomics after SLC25A1 knockdown in Kasumi-1 cells. (L) The change of coenzyme A level detected by metabolomics after SLC25A1 knockdown in Kasumi-1

cells. (M) Palmitic acid supplementation partially rescues impaired proliferation in SLC25A1 KD cells. (N) The heat map showing the change of PG level detected by lipidomics after SLC25A1 knockdown in Kasumi-1 cells. (O) The protein expression of DGAT1 by WB after SLC25A1 knockdown in Kasumi-1 and THP1 cells. (P) The synergistic effect of CTPI2 and DGAT1i (A922500) on inhibiting the growth of THP1.

Supplementary Figure 9. Evaluation of CTPI3 efficacy and safety *in vivo.*

(A) Flow cytometry analysis of apoptosis in Kasumi-1 and THP-1 cells treated with CTPI3 for 48 hours, showing increased apoptosis cell populations compared with controls. Quantification is shown in the adjacent bar graphs. (B) *In vivo* efficacy of CTPI3 in the AE9a mouse model. Representative images of spleen size, H&E staining of spleen sections, and flow cytometry analysis of $GFP^{+}Mac1^{-}$ blasts in bone marrow (BM), spleen (SP) and peripheral blood (PB) indicate a reduction in spleen mass and infiltration of blasts upon CTPI3 treatment. (C) H&E staining of liver, kidney, and brain tissues, indicating no overt toxicity. Detection of HGB and PLT in PB and immunohistochemical staining for cleaved caspase-3 (C-caspase3) in liver, kidney, and brain tissues showing CTPI3 treatment *in vivo* with minimal systemic toxicity.

Supplementary Figure 10. Evaluation of CTPI3's combination effects with venetoclax *in vitro*. (A) Quantification of tricarboxylic acid (TCA) cycle metabolites. Relative levels of α-ketoglutarate, pyruvic acid, oxalic acid, fumaric acid, maleic acid and succinic acid were assessed to determine metabolic changes following CTPI3

treatment. (B) Expression of CPT1A and CPT1C in Kasumi-1 cells treated with CTPI3, venetoclax, or their combination, as assessed by qPCR and Western blotting. (C) Heatmap of targeted metabolomic profiling highlighting changes in fatty acid species and carnitine derivatives following single or combined treatments.

Supplementary Figure 1

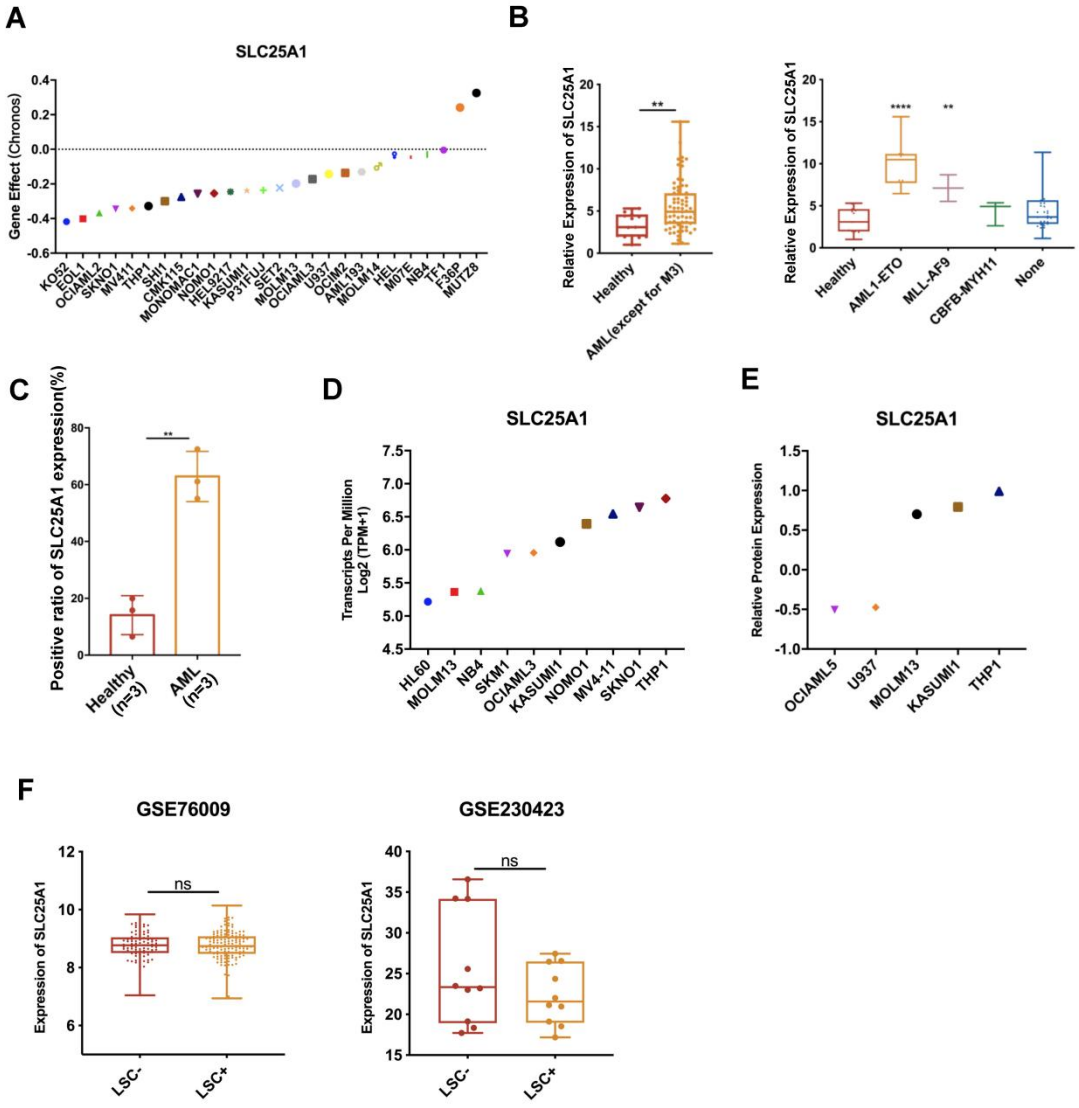

Supplementary Figure 2

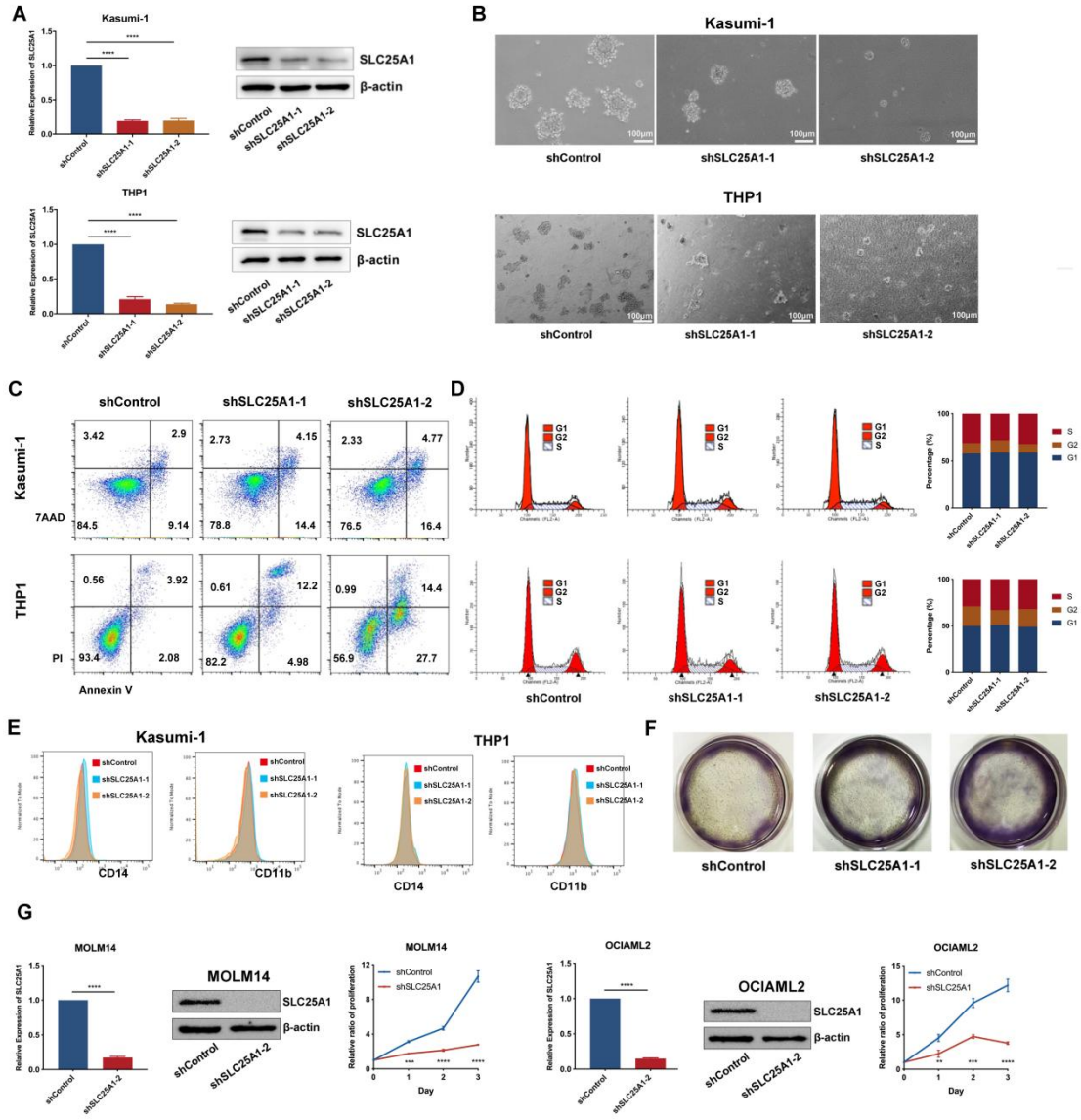

Supplementary Figure 3

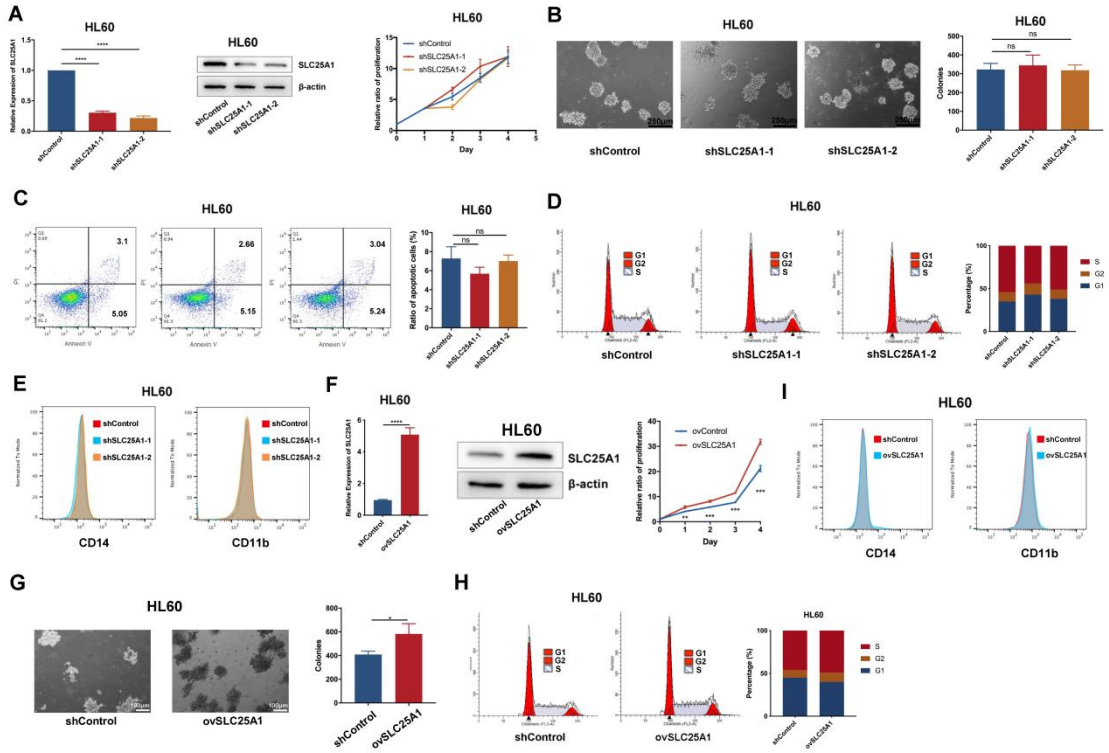

Supplementary Figure 4

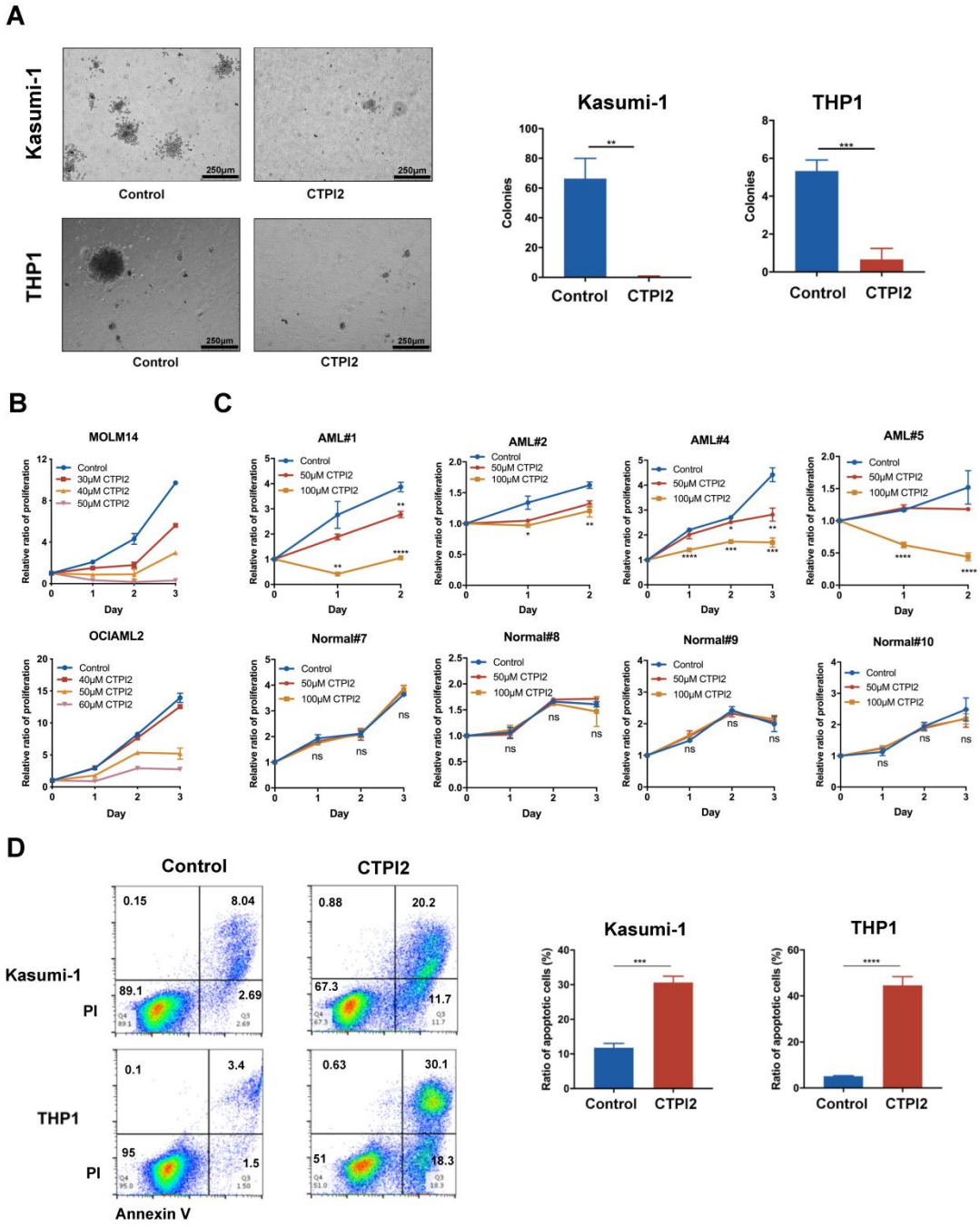

Supplementary Figure 5

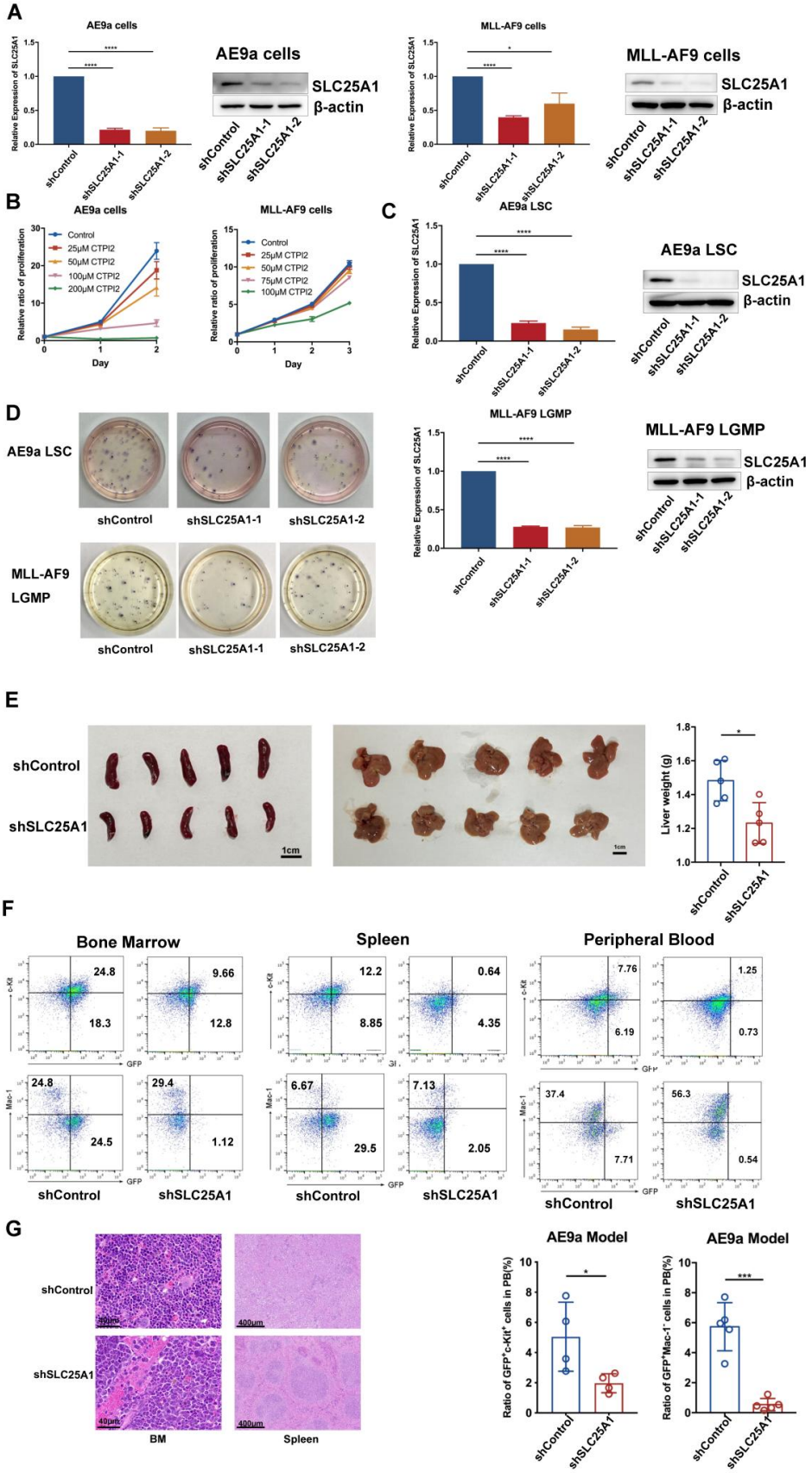

Supplementary Figure 6

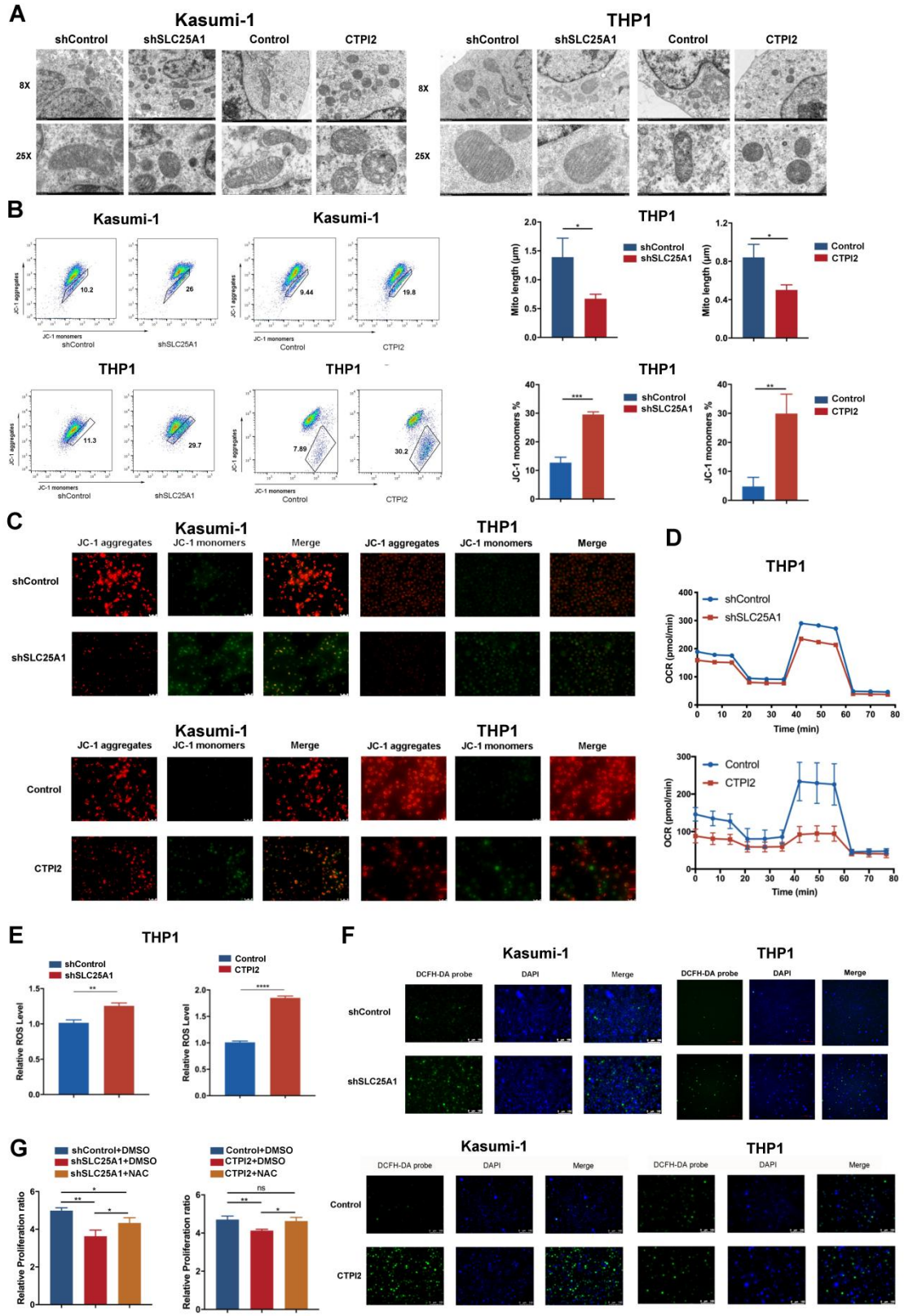

Supplementary Figure 7

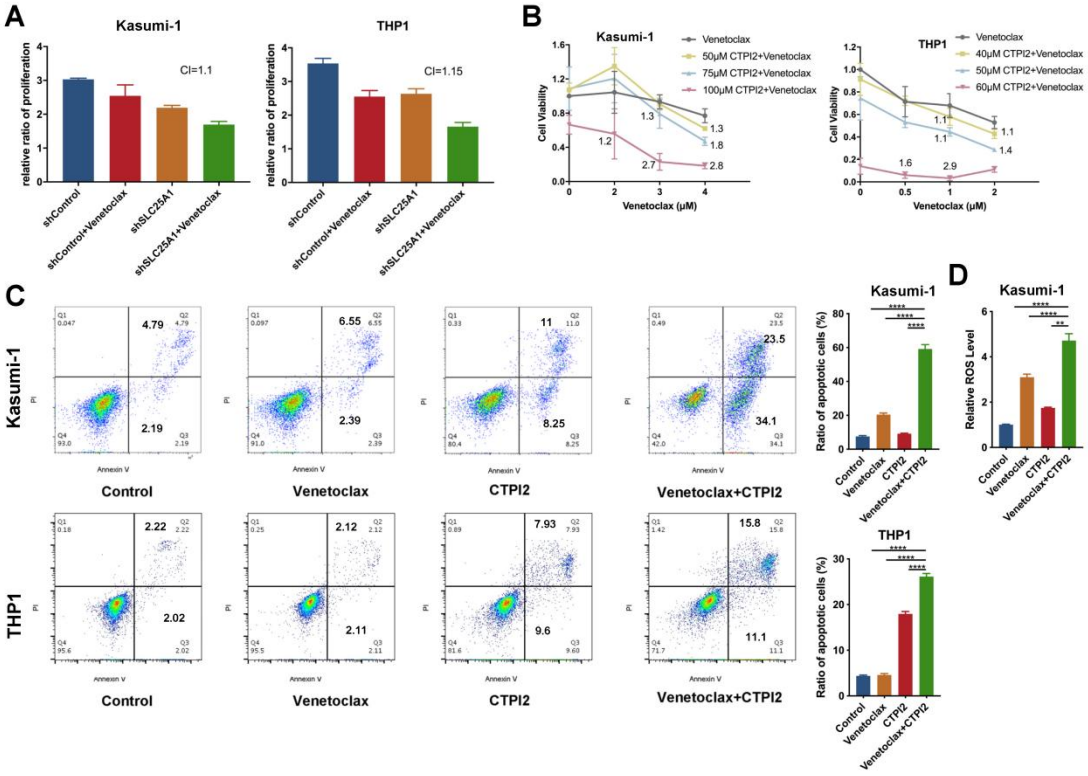

Supplementary Figure 8

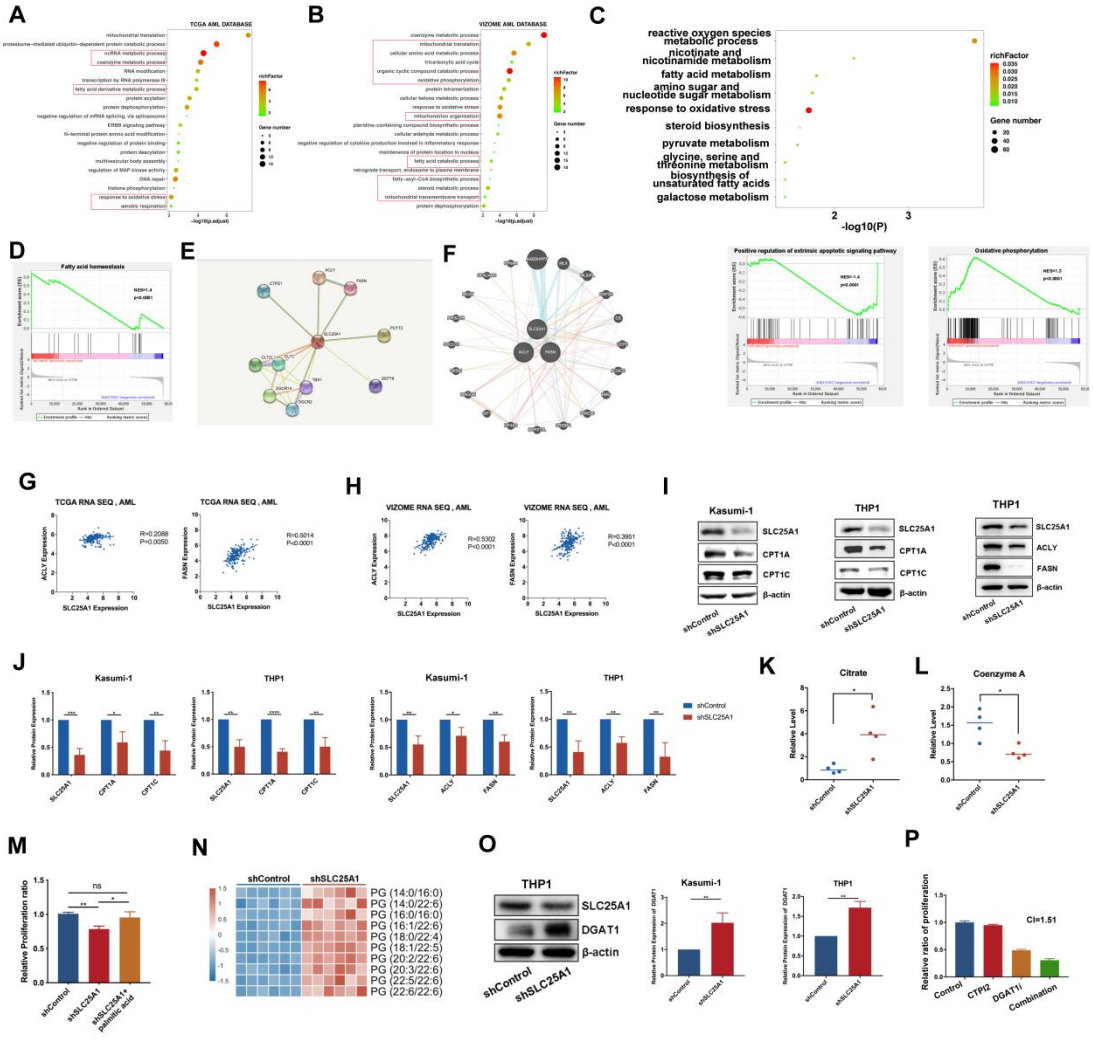

Supplementary Figure 9

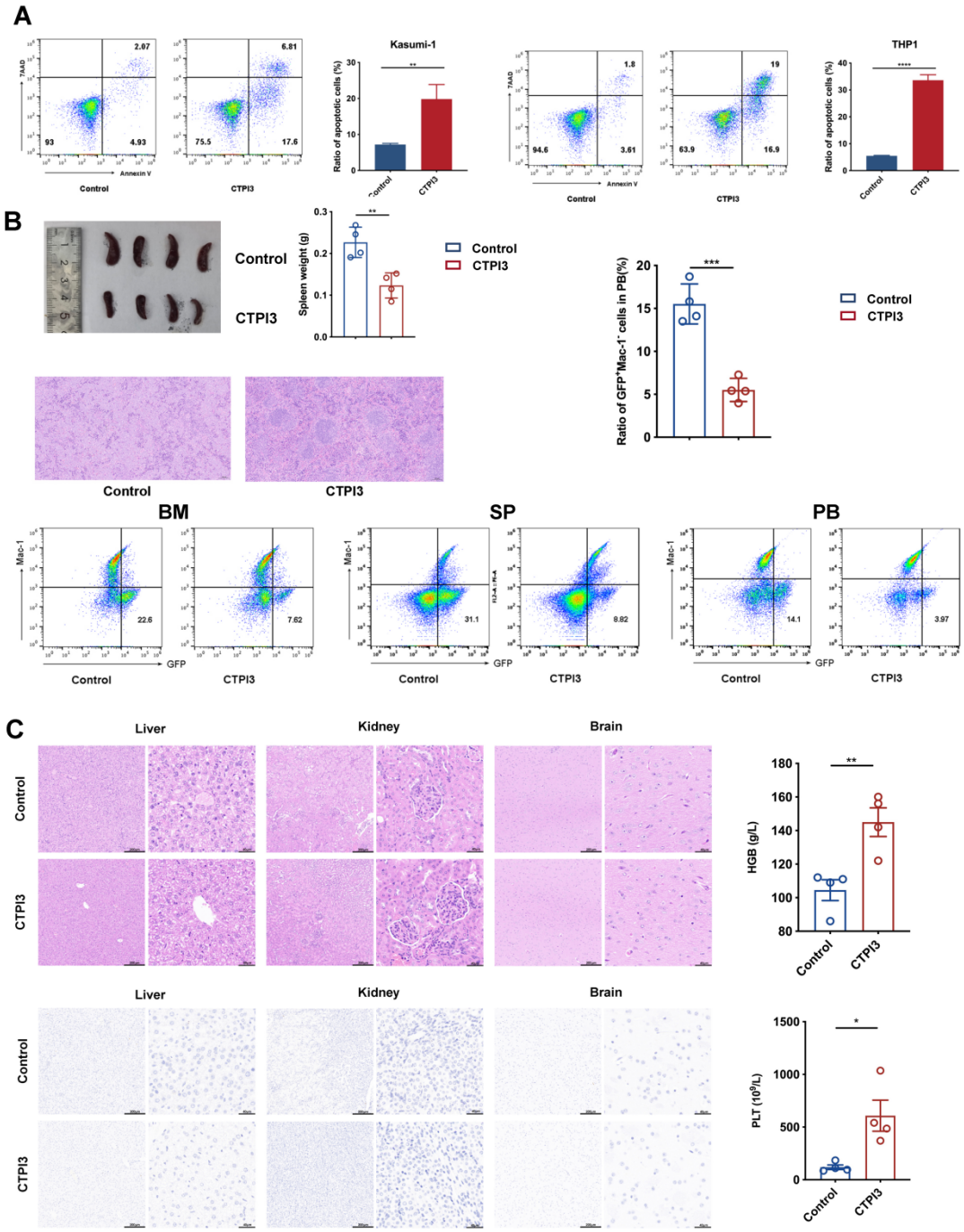

Supplementary Figure 10

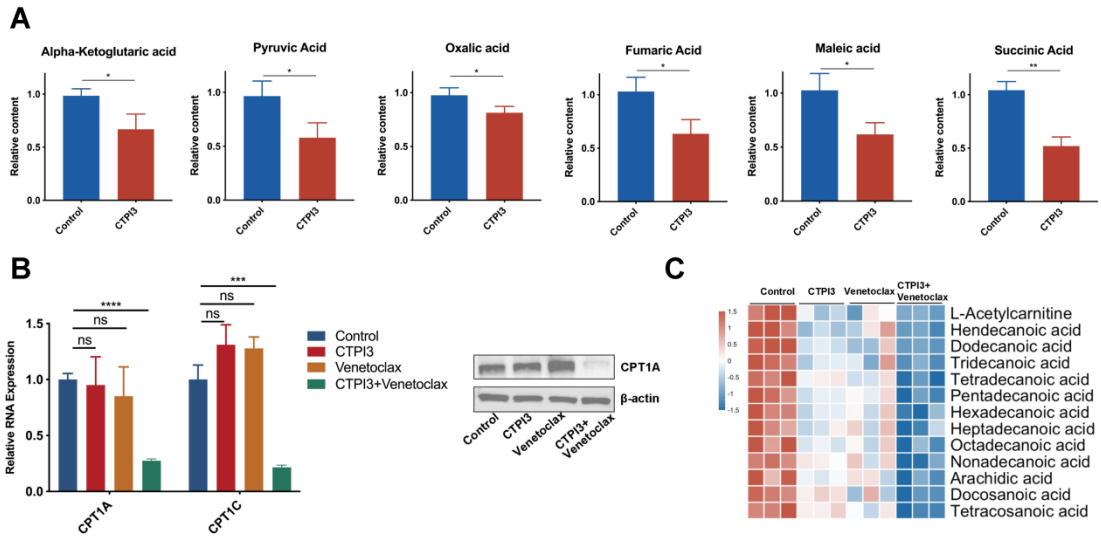

Supplemental Methods

Cell lines

The human AML cell lines Kasumi-1, THP1, HL60, MOLM14, and OCIAML2 were purchased from the Chinese Academy of Sciences cell bank (Shanghai, China). Mouse AE9a, AE9a LSC, MLL-AF9, and MLL-AF9 LGMP AML cells were obtained from Lan Wang, Shanghai Institute of Nutrition and Health. Kasumi-1, THP1, HL60, MOLM14, OCIAML2, and AE9a cells were maintained in RPMI-1640 medium containing 10% fetal bovine serum (FBS). AE9a LSC, MLL-AF9, and MLL-AF9 LGMP cells were maintained in RMPI 1640 medium containing 10% FBS, 50 ng/mL SCF, 10 ng/mL interleukin 3（IL-3) and 10 ng/mL interleukin 6 (IL-6).

Patient samples

Healthy donor samples and AML patient samples were obtained from the First Affiliated Hospital of China Medical University, with informed consent. The research was approved by the ethics committee of The First Hospital of China Medical University ([2022] Number174). Mononuclear cells (MNCs) were isolated from primary bone marrow cells using Ficoll centrifugation and maintained in RPMI-1640 medium containing 20% FBS and medium from 5637 cells.

Mice

Female C57BL/6N mice (6–8 weeks old) were purchased from Beijing Vital River Laboratory Animal Technology. All mice were bred in laminar flow cabinets under

specific pathogen-free conditions in the Laboratory Animal Center of China Medical University. Animal experiments were carried out in accordance with the China Medical University Animal Care and Use Committee guidelines.

Data Collection

Transcriptome sequencing data of 542 AML patients and 74 healthy volunteers were collected from GSE13159 (https://www.ncbi.nlm.nih.gov/geo/query/acc.cgi?acc=GSE13159). Clinical information and transcriptome sequencing data from The Cancer Genome Atlas (TCGA) in cases of AML patients were downloaded from https://xenabrowser.net. Clinical information along with transcriptome sequencing data of VIZOME were downloaded from https://www.vizome.org/ and https://www. cbiopportal.org/. AML patients' clinical information and transcriptome sequencing data of ohsu-AML were downloaded from https://www. cbiopportal.org/.

Mitochondrial membrane potential

The mitochondrial membrane potential of treated Kasumi-1 and THP1 cells was detected using a JC-1 kit with flow cytometry or fluorescence microscopy, according to the manufacturer's protocol.

Cell differentiation assay

AML cells were stained with CD11b and CD14 antibody and detected using flow cytometry.

Hematoxylin and eosin staining

Mice tissues were fixed in 4% paraformaldehyde, embedded in paraffin, and cut into 4 μM sections. The dried sections were then dewaxed and rehydrated. Hematoxylin was used to stain the nucleus, and eosin was used to stain cytoplasm. The sections were finally dehydrated and sealed.

Cell cycle assay

Cell cycle was detected using a KeyGEN Cell Cycle Analysis Kit, according to the manufacturer's protocol.

RNA extraction and reverse-transcription quantitative PCR (RT-qPCR)

Total RNA was extracted using TRIizol reagent according to manufacturer's protocol [1]. cDNA was acquired by reverse transcribing total RNA using a Prime-Script RT Master Mix Kit. RT-qPCR was performed with TB Green Premix Ex Taq II. The PCR primer sequences are list in Supplementary Table 1.

Immunohistochemistry

Bone marrow MNCs were fixed in 4% paraformaldehyde, embedded in paraffin, cut into 4 μM sections, and immunostained with streptavidin-biotin.

Western blot

Total proteins were extracted using whole-cell lysis buffer and the concentration was quantified by bicinchoninic acid assay. For each sample, 20 μg protein was loaded, electrophoresed, transferred to a polyvinylidene difluoride membrane, and blocked

with 5% skimmed milk. The membranes were then incubated with primary antibodies overnight at 4°C, followed by secondary antibodies for 1 h at 25°C. Protein expression was visualized using enhanced chemiluminescence reagents.

Cell proliferation

Cell proliferation was determined using a Cell Counting Kit-8 (CCK8), with 8×10^3 cells in each well of a 96-well plate, with 100 μL medium. CCK8 reagent (10 μL) was added directly to the plates and incubated for 2 h. The absorbance at 450 nm was then recorded. For trypan blue staining, 1×10^5 cells were plated in each well of a 6-well plate with 2 mL medium, and 10 μL of trypan blue reagent was mixed with 10 μL of medium for 3 min.

Colony-formation assay

For colony-formation assay, 5×10^3 cells were plated in 6-well plates with 1 mL Methocult GF-H4435 or Methocult GF-M3434 medium for 7–14 days.

Cell apoptosis assay

Cell apoptosis was detected using an Apoptosis Detection Kit (BD Biosciences), according to the manufacturer's protocol [1].

ROS detection assay

Cellular ROS were detected using a DCFH-DA kit with flow cytometry or fluorescence microscopy, according to the manufacturer's protocol [2].

Untargeted metabolomics

Kasumi-1 cells were infected with lentivirus expressing shRNA against SLC25A1 (scrambled shRNA as control). The metabolites were then extracted from the cells and subjected to ultra-high-performance liquid chromatography–tandem mass spectrometry (UHPLC-MS/MS) using a Vanquish UHPLC system (ThermoFisher, Germany) coupled with an Orbitrap Q ExactiveTM HF mass spectrometer (Thermo Fisher) at Novogene Co., Ltd. (Beijing, China). The raw data files generated by UHPLC-MS/MS were processed using Compound Discoverer 3.1 (CD3.1, ThermoFisher) to perform peak alignment, peak picking, and quantitation for each metabolite. These metabolites were annotated using the Kyoto Encyclopedia of Genes and Genomes (https://www.genome.jp/kegg/pathway.html), HMDB d (https://hmdb.ca/ metabolites), and LIPIDMaps databases (http://www.lipidmaps.org/).

References

1. Hu C, Chen B, Li Z, et al. Targeting UHRF1-SAP30-MXD4 axis for leukemia initiating cell eradication in myeloid leukemia. Cell research. 2022;32(12):1105-1123.

2. Shen S, Yan Z, Wu J, et al. Characterization of ROS Metabolic Equilibrium Reclassifies Pan-Cancer Samples and Guides Pathway Targeting Therapy. Frontiers in oncology. 2020;10(581197.

Supplemental Tables

Table S1 GO analysis of RNA sequence- see excel file

Table S2 GO analysis of metabolomics- see excel file

Table S3 Antibodies and Reagents

Antibody	**Brand**	**Catalog Number**
GAPDH Monoclonal antibody	PTG	60004-1
β-actin Monoclonal antibody	PTG	66009-1-Ig
HRP-conjugated Affinipure Goat Anti-Mouse IgG(H+L)	PTG	SA00001-1
HRP-conjugated Affinipure Goat Anti-Rabbit IgG(H+L)	PTG	SA00001-2
SLC25A1 Polyclonal antibody	PTG	15235-1-AP
ACLY Polyclonal antibody	PTG	15421-1-AP
FASN Polyclonal antibody	PTG	10624-2-AP
CPT1A Polyclonal antibody	PTG	15184-1-AP
CPT1C Monoclonal antibody	PTG	66072-1-Ig
DGAT1 Recombinant antibody	PTG	82945-1-RR
BD Pharmingen™ APC Mouse Anti-Human CD117 (c-Kit)	BD	567127
BD Pharmingen™ PE Mouse Anti-Human CD11b	BD	555388
Reagents	**Brand**	**Catalog Number**
Fetal Bovine Serum, qualified, heat inactivated, United States	Gibco	16140071
Penicillin-Streptomycin-Glutamine (100X)	Gibco	10378016

RPMI 1640 Medium, GlutaMAX™ Supplement	Gibco	61870036
RIPA Lysis Buffer	Beyotime Biotechnology	P0013K
Immobilon-P PVDF Membrane	Millipore	IPVH00010
Chemistar™ High-sig ECL Western Blotting Substrate	Tanon	180-5001
TRIzol™ Reagent	Invitrogen	15596026
PrimeScript™ RT Master Mix (Perfect Real Time)	TAKARA	RR036Q
TB Green® Premix Ex Taq™ II (Tli RNaseH Plus)	TAKARA	RR820Q
BD Annexin V-FITC Apoptosis Detection Kit	BD	556547
Cell Counting Kit-8	Dojindo	CK04
MethoCult H4100	STEMCELL	04100
MethoCult SF H4436	STEMCELL	04436
MethoCult GF M3434	STEMCELL	03434
Mitochondrial membrane potential detection kit (JC-1)	Beyotime Biotechnology	C2006
ROS detection kit	Beyotime Biotechnology	S0033S
Citric acid	Selleck	S5761
Palmitic acid	Selleck	S3794
Software and equipment	**Brand**	
Prism 7	GraphPad	
R version 3.4.2	R Project for Statistical Computing	

Table S4 Primer sequence

SLC25A1 RNA-F	ACGGGGTTAGGGAGATTGTG
SLC25A1 RNA-R	GCCTGCAATAGCTCCGAAGA
GAPDH RNA-F	GTCTCCTCTGACTTCAACAGCG
GAPDH RNA-R	ACCACCCTGTTGCTGTAGCCAA
mouse SLC25A1 RNA-F	GGAGAGGACTATTGTGCGGTCT
mouse SLC25A1 RNA-R	CCCGTGGAAAAATCCTCGGTAC
mouse GAPDH RNA-F	CATCACTGCCACCCAGAAGACTG
mouse GAPDH RNA-R	ATGCCAGTGAGCTTCCCGTTCAG